Journal of Magnetic Resonance 307 (2019) 106584

Contents lists available at ScienceDirect

Journal of Magnetic Resonance

journal homepage: www.elsevier.com/locate/jmr

Larmor frequency dependence on structural anisotropy of magnetically heterogeneous media

Alexander Ruh [a,b], Valerij G. Kiselev [a,*]

[a] Medical Physics, Dept. of Radiology, Medical Center – University of Freiburg, Faculty of Medicine, University of Freiburg, Germany
[b] Dept. of Radiology, Feinberg School of Medicine, Northwestern University, Chicago, IL, United States

ARTICLE INFO

Article history:
Received 8 June 2019
Revised 21 August 2019
Accepted 22 August 2019
Available online 24 August 2019

Keywords:
Structural anisotropy
Magnetic susceptibility
Phase contrast
Tissue microstructure
Lorentz cavity

ABSTRACT

The effect of anisotropic magnetic microstructure on the measurable Larmor frequency offset is investigated in media with heterogeneous magnetic susceptibility using Monte Carlo simulations. The focus is on the transition between the regimes of fast and slow diffusion of NMR-reporting molecules. Simulations demonstrate a perfect agreement with the previously developed analytic theory for fast diffusion. Beyond this regime, the frequency offset shows a pronounced dependence on the medium microarchitecture and the diffusivity of NMR-reporting spins in relation to the magnitude of the susceptibility-induced magnetic field.

1. Introduction

Precise signal phase measurements [1–3] initiated a still ongoing discussion of the microstructural correlates of the proton precession frequency in brain white matter [4–16]. In a broader view, the question is about the averaged Larmor frequency of an ensemble of spins, moving in a magnetically heterogeneous medium, for instance, containing microscopic inclusions with a distinct magnetic susceptibility (e.g. the matrix in a porous medium or biological cells). While the case of fast moving spins, the so-called *diffusion narrowing regime* (DNR), remains in the discussion focus, a few studies addressed the opposite regime of negligible diffusion, the so-called *static dephasing regime* (SDR) [17–19]. To the best of our knowledge there is a single study of the transition between these limiting cases for the case of isotropic media [19].

In the present study this transition is investigated *in silico* for anisotropic media. Our simulations demonstrate the importance of the *structural anisotropy* of the medium microarchitecture. For a given medium microstructure, the transition is governed by a combined parameter describing the typical phase accumulation by a spin diffusing over the characteristic microstructural length scale. The simulations also validate the recently developed theory for anisotropic media in the DNR [20].

2. Problem formulation

We consider media with impermeable, NMR-invisible inclusions with the isotropic magnetic susceptibility χ relative to the surrounding NMR-visible fluid (Fig. 1). Exposed to the external field $\mathbf{B}_0$, the inclusions create a local Larmor frequency shift $\Omega(\mathbf{r})$, which is the most straightforward to calculate in terms of the Fourier transformed quantities,

$$\Omega(\mathbf{k}) = \delta\Omega\, Y(\mathbf{k})\, \nu(\mathbf{k}), \quad \delta\Omega = 4\pi\gamma|\mathbf{B}_0|\chi, \tag{1}$$

where the cgs system is used, γ is the proton gyromagnetic ratio and $\nu(\mathbf{k})$ the Fourier transform of $\nu(\mathbf{r})$, the indicator function that is unity inside the susceptibility inclusions and zero otherwise. Throughout this paper we use the same letters for real-space and Fourier-transformed quantities; the argument is always given explicitly to avoid confusion. The function $Y(\mathbf{k})$ is proportional to the elementary dipole field,

$$Y(\mathbf{k}) = \frac{1}{3} - \frac{k_3^2}{k^2}, \tag{2}$$

where the third direction is selected along the main magnetic field. In what follows, the local Larmor frequency, $\Omega(\mathbf{r})$, is referred to as *the field*.

The objective of this work is to find how this heterogeneous field is averaged in the overall signal from the sample giving rise to the observed Larmor frequency shift $\overline{\Omega}$. Since the averaging in the near region depends on the dynamics of moving spins, we fol-

* Corresponding author at: Medical Physics, Department of Radiology, Medical Center – University of Freiburg, Killianstr. 5a, 79106 Freiburg, Germany.
E-mail address: kiselev@ukl.uni-freiburg.de (V.G. Kiselev).

https://doi.org/10.1016/j.jmr.2019.106584
1090-7807/

low the original idea of Lorentz [21] separating the sample in a far region with an easily calculable contribution to the frequency shift and a near region where the field averaging depends on details of spin motion, Fig. 1. The transition from the near to the far region is encompassed by the *mesoscopic sphere* [22,19,16] to which the present analysis exclusively applies. In real experiments, the field created by the rest of the sample should be added as illustrated in Fig. 1.

In general, the spin dynamics in the near region are controlled by the parameter [19]

$$\alpha = \frac{\delta\Omega\,\ell_c^2}{D}, \tag{3}$$

where D is the isotropic diffusivity in the fluid and ℓ_c the microstructural correlation length in the medium; for dense packings of compact objects, this length is defined by their size. The controlling parameter α is the typical phase acquired by a spin diffusing past a single correlation length. In the DNR, $\alpha \ll 1$, the field averaging can be performed analytically for a broad class of inclusions' shape [19,20],

$$\overline{\Omega} = \langle\Omega\rangle = -\frac{\delta\Omega}{1-\zeta}\int\frac{\mathrm{d}^3k}{(2\pi)^3}\,\Gamma(\mathbf{k})\,Y(\mathbf{k}), \tag{4}$$

where ζ is the volume fraction of the susceptibility inclusions with $\zeta = \langle v(\mathbf{r})\rangle$, and $\Gamma(\mathbf{k})$ the Fourier transform of the two-point correlation function of inclusions,

$$\begin{aligned}\Gamma(\mathbf{r}) &= \Big\langle v(\mathbf{r}_0+\mathbf{r})\,v(\mathbf{r}_0)\rangle_{\mathbf{r}_0} - \zeta^2,\\ \Gamma(\mathbf{k}\neq 0) &= \frac{1}{V}\,v(\mathbf{k})\,v(-\mathbf{k}), \quad \Gamma(\mathbf{k}=0) = 0.\end{aligned} \tag{5}$$

This correlation function was considered in detail in Refs. [23,24] and is illustrated in Fig. 2. Note that the so-called "averaged magnetic environment" [13] is tightly related to the correlation function. In the present notations, this quantity is proportional to $\zeta(1-\zeta) - \Gamma(\mathbf{r})$.

When integrated over $\mathbf{k}$, the correlation function, $\Gamma(\mathbf{k})$, gives the variance, $\Gamma(\mathbf{r}=0) = \zeta(1-\zeta)$. This property underlies the general result for the frequency shift induced by parallel cylindrical objects within the mesoscopic sphere,

$$\overline{\Omega} = -\frac{\zeta}{2}\left(\cos^2\theta - \frac{1}{3}\right)\delta\Omega, \tag{6}$$

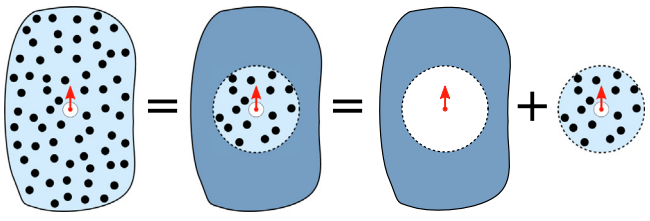

Fig. 1. A sample with a microscopic magnetic structure and the decomposition of its magnetization for calculating the magnetic field at the position of an NMR-reporting spin (red arrow). The heterogeneous magnetization is shown as inclusions (black dots) with a magnetic susceptibility, χ, different from that of the surrounding fluid (light blue). The first equality: The sample can be divided into a far and a spherical near region, the *mesoscopic sphere* (the sphere size is greatly exaggerated in the image). The far region contributes a field induced by its average (homogenized) susceptibility (darker blue). The second equality: The field at the spin's position is the sum of two contributions induced by the far region with excluded mesoscopic sphere and the mesoscopic sphere. While the former is governed by the macroscopic averaged magnetic susceptibility, the latter depends on the medium microarchitecture. The small empty sphere stands for the classical Lorentz sphere in the NMR-reporting fluid. (For interpretation of the references to colour in this figure legend, the reader is referred to the web version of this article.)

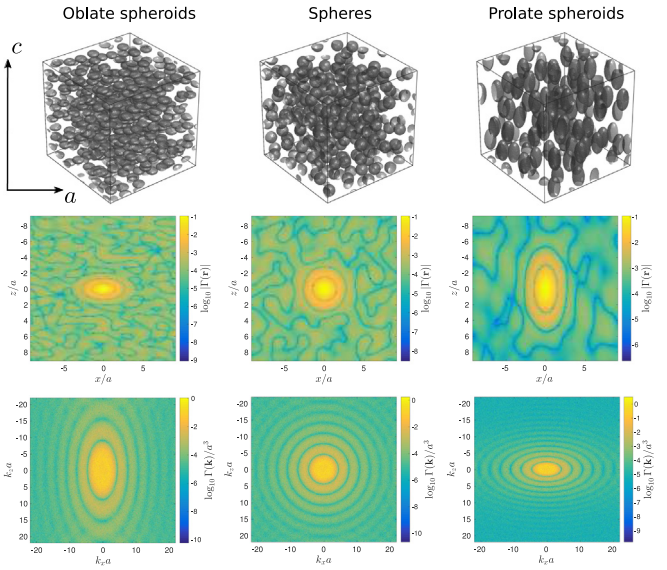

Fig. 2. Top row: Examples of simulated media consisting of identical magnetic susceptibility inclusions shaped as oblate spheroids (axes ratio $c/a = 0.5$), spheres and prolate spheroids ($c/a = 2$); a is the same for all three. The visualization shows a quarter of the simulation box in each dimension. Middle row: Sections of the correlation functions by planes parallel to the symmetry axis. The color indicates the value of $\log_{10}|\Gamma(\mathbf{r})|$. Bottom row: The corresponding Fourier-transformed correlation functions shown as $\log_{10}(\Gamma(\mathbf{k})/a^3)$. (For interpretation of the references to colour in this figure legend, the reader is referred to the web version of this article.)

where θ is the angle between the objects' axis and the main field [20,16]. In overall cylindrical samples, this term cancels the well-known contribution of the far region shown with the first term on the right-hand side in Fig. 1.

In the opposite case, the SDR with $\alpha \gg 1$, analytical results are available for spherical and cylindrical inclusions with a low overall volume fraction, $\zeta \ll 1$ [17]. In an *in silico* study [19], the transition between the extreme regimes was investigated for isotropic media made with spherical inclusions. In the present study, such transition is analyzed for structurally anisotropic media made with non-spherical objects while the objects' material by itself is isotropic.

3. Methods

Disordered three-dimensional media consisting of non-overlapping, identical inclusions with a distinct magnetic susceptibility were generated using random sequential addition with periodic boundary conditions in all three spatial directions (Fig. 2). The volume fraction of inclusions was $\zeta = 0.15$. The inclusions had the form of spheroids with the semiaxes c, a, a with a given aspect ratio c/a. Different media were generated for c/a selected as powers of 2 in the range from 1/8 to 16. To obtain structural anisotropy, the orientation of the principal axis, c, was restricted to a narrow cone with solid angle 0.008 sr; in isotropic media, spheroids were randomly oriented. The correlation length within the media, ℓ_c, was defined as the radius of a sphere with the same volume as the spheroids.

The generated media were sampled on a 1024^3 cubic grid for numerical computations of the field and successive Monte Carlo (MC) simulations. The inclusion size was chosen from $a = 7\Delta x$ for prolate to $a = 28\Delta x$ for oblate spheroids to keep their volume comparable, where Δx was the grid spacing. The local precession frequency was calculated according to a discretized version of Eq.

(1) with the $\mathbf{k} = 0$ component explicitly set to zero [19,16]. For media consisting of oriented spheroids, the magnetic field was generated twice, parallel and perpendicular to the object orientation (the c axis).

Diffusion was simulated by random hopping on the grid with periodic boundary conditions in all directions [19]. Random walkers were initialized outside the inclusions and kept there by prohibiting the penetration inside. This was implemented by rejecting the hops inside an inclusion and waiting till the next attempt to move. All random walkers travelled independently of each other. The complex-valued free induction decay signal was calculated as the mean of accumulated phase factors of individual random walkers at every time point. The number of random walkers was $N = 10^6$ for fast diffusion and was increased to 10^7 for $\alpha > 100$, Eq. (3), to compensate for less diffusion averaging in this regime. The frequency shift, $\overline{\Omega}$, was determined by the maximum of the spectral line obtained from the Fourier transformation of the signal time course. In order to reduce the noise, the time domain signals were only considered until they became noise-dominant. This time moment was defined by the first increase in the signal magnitude in the time domain where it was below 0.1% of the initial signal. The rest of the time axis was zero filled to obtain interpolated spectra [19].

Note that in spite of the apparent difference in geometry, the cubic simulation box with periodic boundary conditions is equivalent to the mesoscopic sphere [19]. This follows from the equivalence of all points in such a volume and the nulling of the magnetic field from homogeneously distributed magnetization, the $\mathbf{k} = 0$ component. This equivalence enables considering each random walker as initiated in the center of its own mesoscopic sphere as it is implied by theory.

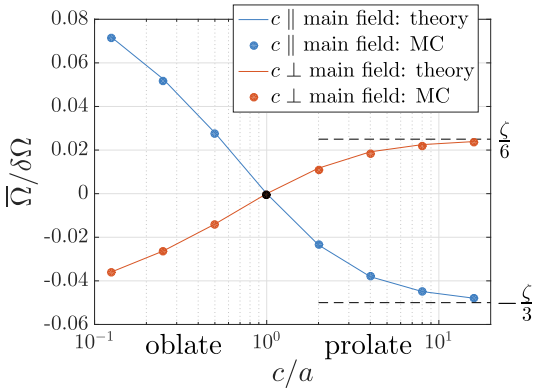

Fig. 3. The frequency shift, $\overline{\Omega}/\delta\Omega$, for fast diffusion ($\delta\Omega\ell_c^2/D \lesssim 4$) for different media, characterized by their aspect ratio c/a (abscissa) for parallel (blue) and perpendicular (red) orientations to the main field. Solid lines show the results of numerical integration of the correlation function according to Eq. (4). This prediction does not involve any parameter fitting. Circles show results of Monte Carlo simulations in the same media demonstrating an excellent agreement with theory. Note the black circle showing zero frequency shift for isotropic (spherical) inclusions ($c/a = 1$). When the prolate spheroids get longer, the frequency shift approaches the theoretically calculable limits of infinitely long cylinders, $\theta = 0$ and $\theta = \pi/2$ in Eq. (6) (dashed lines). (For interpretation of the references to colour in this figure legend, the reader is referred to the web version of this article.)

4. Results

We first investigated the microstructure dependence of the frequency shift for fast diffusion in the limit of DNR. Fig. 3 shows the result of Monte Carlo simulations for various aspect ratios of spheroids. Comparison with the deterministic theory expressed by Eq. (4) demonstrates a perfect agreement without any parameter fitting.

The transition from the DNR to the SDR is illustrated in Fig. 4. The result shows a pronounced dependence on the medium structure and the value of the controlling parameter α, Eq. (3). The results for spheroids with random orientation are very close to that for spheres. For the DNR, this follows from Eq. (4), which is not sensitive to the origin of an isotropic correlation function, either due to the spherical inclusions or randomized non-spherical ones. A light deviation from this equivalence is observed in the SDR.

The α-dependence flattens out when the medium approaches the case of long cylinders parallel to the main magnetic field. The limiting α-independent value is $-\zeta/3$ according to Eq. (6) with $\theta = 0$. This corresponds [20] to the well-known fact that a bunch of cylinders parallel to the main field does not create any field in the space between cylinders. In such a sample, the volume external to the mesoscopic sphere (the first term on the right-hand side of the graphical equation shown in Fig. 1) has a cylindrical shape with a void, which results in the precisely opposite contribution. Since this contribution is governed by the averaged magnetic susceptibility, it is insensitive to the microstructure and so is the compensating field of the mesoscopic sphere.

5. Discussion

This study provides a validation for the recently obtained analytical expression, Eq. (4), describing the frequency shift in the diffusion narrowing regime. Dependence of the precession frequency on the microstructure in this regime was first discussed in

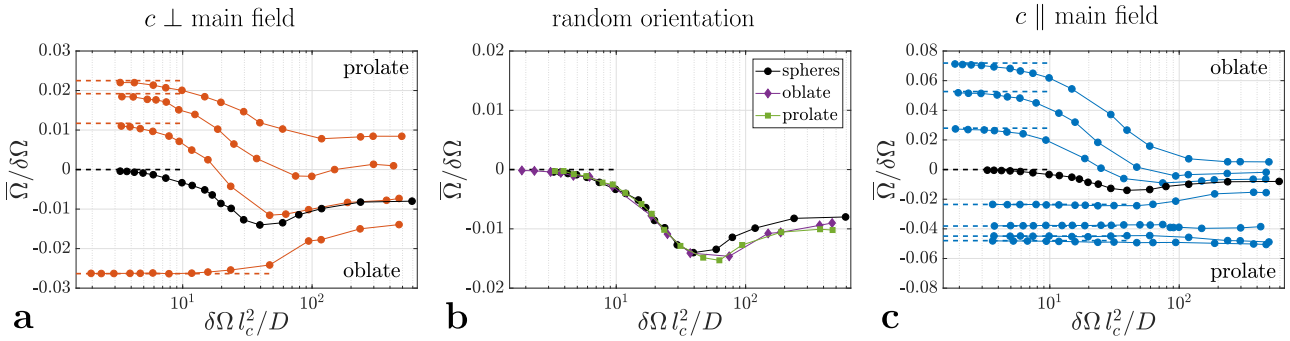

Fig. 4. The frequency offset shows a pronounced dependence on the regime-controlling parameter $\alpha = \delta\Omega\ell_c^2/D$, Eq. (3) (abscissas) and the inclusions's shape and orientation. For small values of α all results approach the theoretical DNR limit, Eq. (4) (dashed lines). Results for spherical inclusions are reproduced in black in all panels. **a**: Inclusions with coherent orientations with the symmetry axis c perpendicular to the main field. The inclusions' shape is changed from prolate to oblate spheroids (top to bottom). **b**: Inclusions with $c/a = 0.5$ and 2 with random orientations. **c**: The media from panel (**a**) plus three more for the field parallel to the symmetry axis (all media from Fig. 3). The result for the most prolate inclusions approaches the value for long cylinders in the mesoscopic sphere, $-\zeta/3 = -0.05$.

the context of NMR in anisotropic solutions and liquid crystals [25–28]. A pronounced precession frequency dependence on the microstructure was obtained using MC simulations for the model of multiple sclerosis in which the same amount of magnetic material was redistributed from hollow cylinders representing the intact myelin sheets to isotropically distributed debris [5]. The dependence on microstructure was confirmed in the following theoretical studies [6,11,13] and discussed in a review series [12–16].

In more detail, the present study deals with structurally anisotropic media in which the anisotropy is achieved exclusively by the form of inclusions, while the magnetic susceptibility of inclusions' material is isotropic. According to Eq. (4), possible anisotropy in the arrangement of susceptibility inclusions enters via a single quantity, the inclusions' correlation function, which represents the medium structure in a unified way. We did not consider the effect of molecular-level anisotropy described by the magnetic susceptibility tensor of the inclusions' material [29–31,6,12,13]; a generalization of Eq. (4) for this case was obtained recently [20].

In the opposite limiting case of the static dephasing, the precession frequency also depends on the microstructure [17,32] as does the transition between the DNR and the SDR. The macroscopically isotropic samples show similar behavior, regardless whether they are composed with isotropic objects [19] or become isotropic upon averaging over the orientation ofanisotropic ones. While the mechanism of such reduction is known in the DNR [20], what are the effect-defining features in the SDR remains to be understood.

The obtained results are applicable to porous media with NMR-invisible matrix and NMR-reporting fluid filling the pores. In the biomedical context, they can be rather a part of a more complex overall picture that includes multiple tissue compartments.

Acknowledgement

This work was supported by the German Research Foundation (DFG), grant KI 1089/6-1.

References

[1] A.M. Abduljalil, P. Schmalbrock, V. Novak, D.W. Chakeres, Enhanced gray and white matter contrast of phase susceptibility-weighted images in ultra-high-field magnetic resonance imaging, J. Magn. Reson. Imag. 18 (2003) 284–290, https://doi.org/10.1002/jmri.10362.
[2] J.H. Duyn, P. van Gelderen, T.-Q. Li, J.A. de Zwart, A.P. Koretsky, M. Fukunaga, High-field MRI of brain cortical substructure based on signal phase, Proc. Natl. Acad. Sci. USA 104 (2007) 11796–11801, https://doi.org/10.1073/pnas.0610821104.
[3] J.P. Marques, R. Maddage, V. Mlynarik, R. Gruetter, On the origin of the MR image phase contrast: an in vivo MR microscopy study of the rat brain at 14.1 T, NeuroImage 46 (2009) 345–352, https://doi.org/10.1016/j.neuroimage.2009.02.023.
[4] X. He, D.A. Yablonskiy, Biophysical mechanisms of phase contrast in gradient echo MRI, Proc. Natl. Acad. Sci. USA 106 (2009) 13558–13563, https://doi.org/10.1073/pnas.0904899106.
[5] D.A. Yablonskiy, J. Luo, A.L. Sukstanskii, A. Iyer, A.H. Cross, Biophysical mechanisms of MRI signal frequency contrast in multiple sclerosis, Proc. Natl. Acad. Sci. USA 109 (2012) 14212–14217, https://doi.org/10.1073/pnas.1206037109.
[6] A.L. Sukstanskii, D.A. Yablonskiy, On the role of neuronal magnetic susceptibility and structure symmetry on gradient echo MR signal formation, Magn. Reson. Med. 71 (2014) 345–353, https://doi.org/10.1002/mrm.24629.
[7] J.H. Duyn, Frequency shifts in the myelin water compartment, Magn. Reson. Med. 71 (2014) 1953–1955, https://doi.org/10.1002/mrm.24983.
[8] D.A. Yablonskiy, A.L. Sukstanskii, Biophysical mechanisms of myelin-induced water frequency shifts, Magn. Reson. Med. 71 (2014) 1956–1958, https://doi.org/10.1002/mrm.25214.
[9] J.H. Duyn, T.M. Barbara, Sphere of Lorentz and demagnetization factors in white matter, Magn. Reson. Med. 72 (2014) 1–3, https://doi.org/10.1002/mrm.25021.
[10] D.A. Yablonskiy, X. He, J. Luo, A.L. Sukstanskii, Lorentz sphere versus generalized Lorentzian approach: what would lorentz say about it?, Magn Reson. Med. 72 (2014) 4–7, https://doi.org/10.1002/mrm.25230.
[11] D.A. Yablonskiy, A.L. Sukstanskii, Generalized Lorentzian tensor approach (GLTA) as a biophysical background for quantitative susceptibility mapping, Magn. Reson. Med. 73 (2015) 757–764, https://doi.org/10.1002/mrm.25538.
[12] D.A. Yablonskiy, A.L. Sukstanskii, Effects of biological tissue structural anisotropy and anisotropy of magnetic susceptibility on the gradient echo MRI signal phase: theoretical background, NMR Biomed. 30 (2017) e3655, https://doi.org/10.1002/nbm.3655.
[13] J.H. Duyn, J. Schenck, Contributions to magnetic susceptibility of brain tissue, NMR Biomed. 30 (2017) e3546, https://doi.org/10.1002/nbm.3546.
[14] J.H. Duyn, Studying brain microstructure with magnetic susceptibility contrast at high-field, NeuroImage 168 (2018) 152–161, https://doi.org/10.1016/j.neuroimage.2017.02.046.
[15] D.A. Yablonskiy, A.L. Sukstanskii, Lorentzian effects in magnetic susceptibility mapping of anisotropic biological tissues, J. Magn. Reson. 292 (2018) 129–136, https://doi.org/10.1016/j.jmr.2018.04.014.
[16] A. Ruh, V.G. Kiselev, Calculation of Larmor precession frequency in magnetically heterogeneous media, Concepts Magn. Reson. Part A e21472 (2019), https://doi.org/10.1002/cmr.a.21472.
[17] D.A. Yablonskiy, E.M. Haacke, Theory of NMR signal behavior in magnetically inhomogeneous tissues: the static dephasing regime, Magn. Reson. Med. 32 (1994) 749–763, https://doi.org/10.1002/mrm.1910320610.
[18] P. Kokeny, Y.C.N. Cheng, H. Xie, A study of MRI gradient echo signals from discrete magnetic particles with considerations of several parameters in simulations, Magn. Reson. Imag. 48 (2018) 129–137, https://doi.org/10.1016/j.mri.2017.12.019.
[19] A. Ruh, H. Scherer, V.G. Kiselev, The Larmor frequency shift in magnetically heterogeneous media depends on their mesoscopic structure, Magn. Reson. Med. 79 (2018) 1101–1110, https://doi.org/10.1002/mrm.26753.
[20] V.G. Kiselev, Larmor frequency in heterogeneous media, J. Magn. Reson. 299 (2019) 168–175, https://doi.org/10.1016/j.jmr.2018.12.008.
[21] H.A. Lorentz, Über die Beziehung zwischen der Fortpflanzungsgeschwindigkeit des Lichtes und der Körperdichte, Ann. Phys. 245 (1880) 641–665, https://doi.org/10.1002/andp.18802450406.
[22] C.J. Durrant, M.P. Hertzberg, P.W. Kuchel, Magnetic susceptibility: Further insights into macroscopic and microscopic fields and the sphere of Lorentz, Concepts Magn. Reson. Part A 18A (2003) 72–95, https://doi.org/10.1002/cmr.a.10067.
[23] D.S. Novikov, V.G. Kiselev, Transverse NMR relaxation in magnetically heterogeneous media, J. Magn. Reson. 195 (2008) 33–39, https://doi.org/10.1016/j.jmr.2008.08.005.
[24] L.M. Burcaw, E. Fieremans, D.S. Novikov, Mesoscopic structure of neuronal tracts from time-dependent diffusion, NeuroImage 114 (2015) 18–37, https://doi.org/10.1016/j.neuroimage.2015.03.061.
[25] A.D. Buckingham, T. Schaefer, W.G. Schneider, Solvent effects in nuclear magnetic resonance spectra, J. Chem. Phys. 32 (1960) 1227–1233, https://doi.org/10.1063/1.1730879.
[26] I. Haller, H.A. Huggins, H.R. Lilienthal, T.R. McGuire, Order-related properties of some nematic liquids, J. Phys. Chem. 77 (1973) 950–954, https://doi.org/10.1021/j100626a020.
[27] P. Palffy-Muhoray, The local electric field in certain anisotropic molecular fluids, Chem. Phys. Lett. 48 (1977) 315–316, https://doi.org/10.1016/0009-2614(77)80322-9.
[28] D.A. Dunmur, R.W. Munn, The shape of the Lorentz cavity and the internal field in anisotropic fluids, Chem. Phys. 76 (1983) 249–253, https://doi.org/10.1016/0301-0104(83)85038-1.
[29] C. Liu, Susceptibility tensor imaging, Magn. Reson. Med. 63 (2010) 1471–1477, https://doi.org/10.1002/mrm.22482.
[30] J. Lee, K. Shmueli, M. Fukunaga, P. van Gelderen, H. Merkle, A.C. Silva, J.H. Duyn, Sensitivity of MRI resonance frequency to the orientation of brain tissue microstructure, Proc. Natl. Acad. Sci. USA 107 (2010) 5130–5135, https://doi.org/10.1073/pnas.0910222107.
[31] S. Wharton, R. Bowtell, Fiber orientation-dependent white matter contrast in gradient echo MRI, Proc. Natl. Acad. Sci. USA 109 (2012) 18559–18564, https://doi.org/10.1073/pnas.1211075109.
[32] W.C. Chen, S. Foxley, K.L. Miller, Detecting microstructural properties of white matter based on compartmentalization of magnetic susceptibility, NeuroImage 70 (2013) 1–9, https://doi.org/10.1016/j.neuroimage.2012.12.032.